

Enhanced performance of MoS₂/SiO₂ field-effect transistors by hexamethyldisilazane (HMDS) encapsulation

Santu Prasad Jana, Shivangi, Suraina Gupta, and Anjan K. Gupta

Department of Physics, Indian Institute of Technology Kanpur, Kanpur 208016, India

(Dated: March 12, 2024)

Scalable methods for improving the performance and stability of a field-effect transistor (FET) based on two-dimensional materials are crucial for its real applications. A scalable method of encapsulating the exfoliated MoS₂ on SiO₂/Si substrate by hexamethyldisilazane (HMDS) is explored here for reducing the influence of interface traps and ambient contaminants. This leads to twenty-five times reduction in trap density, three times decrease in subthreshold swing, three times increase in the peak field-effect mobility and a drastic reduction in hysteresis. This performance remains nearly the same after several weeks of ambient exposure of the device. This is attributed to the superhydrophobic nature of HMDS and the SiO₂ surface hydrophobization by the formation of covalent bonds between the methyl groups of HMDS and silanol groups of SiO₂.

Semiconducting transition metal dichalcogenides (TMDs) [1] provide many advantages when integrated into field effect transistors (FETs) in their atomically thin form. Molybdenum disulfide (MoS₂) has appeared as the most favored and vastly researched semiconducting TMD in recent years due to its natural abundance as well as excellent environmental stability. Its mechanical flexibility, high transparency, thickness-dependent bandgap [2, 3], higher mobility than organic semiconductors and the electrostatic gate control make it a favored candidate for the next-generation nano-electronic devices. MoS₂'s applications have been demonstrated in many devices including transistor [3, 4], logic [5, 6], high-frequency [7], circuit integration [8], photodetector [9] optoelectronic [3, 10], light emitters [11] and photovoltaic cells [12].

Nonetheless, the actual device performance of MoS₂ FETs remain significantly below the intrinsic theoretical limit [13, 14] with the actual devices exhibiting hysteresis and degradation [15, 16] with time, particularly, on exposure to ambient conditions. These traits can be attributed to either charge-traps at the MoS₂/SiO₂ interface [17] or the instability related to the facile adsorption of oxygen and water molecules [18]. Consequently, in long-term, the subthreshold swing (SS) becomes large and the carrier mobility reduces. Passivation of the dielectric interface with MoS₂ and protection of top surface by a capping layer have been tried by many research groups. These include different dielectric and encapsulation layers such as, Al₂O₃, HfO₂, hBN, and PMMA [19–24]. Despite significant improvement, owing to the lack of surface dangling bonds in MoS₂, atomic layer deposition (ALD)-processed oxide capping layers exhibit non-uniform growth leading to partial coverage when the capping layer is ultra-thin. The most remarkable performance is achieved with exfoliated hBN encapsulation but this method is not scalable.

In this paper, we present a facile method, for efficient and scalable interface passivation and top protection, for few-layer MoS₂ with an air-stable and thin organic hex-

amethyldisilazane (HMDS) layer. The performance of an HMDS encapsulated device, operated in ambient conditions, is compared with the un-passivated device operated in vacuum. The HMDS encapsulated device exhibits twenty-five times less slow-trap density leading to negligible hysteresis, three times less sub-threshold swing and three times larger peak value of the field effect mobility as compared to the latter. An exposure to ambient air for 25 days leads to about 10% mobility reduction with negligible hysteresis change. The effectiveness of this passivation and protection method is discussed in terms of HMDS properties.

Acetone and IPA cleaned highly p-doped Si wafers with 300 nm thermal SiO₂ are used as a substrate with the back gate. Single- or few-layer MoS₂ flakes are mechanically exfoliated from natural bulk crystal (from SPI) and transferred to the substrate. This uses the conventional dry transfer method [25] with the PDMS film (Gel film from Gel Pak) as a viscoelastic stamp and an XYZ-micromanipulator attached to an optical microscope. For interface passivation, acetone and isopropyl alcohol cleaned substrates were immersed in a 50:50 mixture of HMDS and acetone for 12-15 hrs followed by pure HMDS spin-coating at 2000 rpm for 45 s prior to the MoS₂ transfer. The source-drain contacts are made using mechanical masking with a 15 μm diameter tungsten wire after aligning the MoS₂ flake underneath it with the help of an optical microscope. This is followed by 50-nm-thick gold film deposition by thermal evaporation. By using mechanical masking, the organic lithography resist is avoided, which can leave residue on MoS₂. For the protection of MoS₂ on top, a second HMDS layer was spin coated after the gold contact deposition.

Figure 1(a) shows the optical image of the few-layer MoS₂ FET with HMDS encapsulation and gold contacts. Since the HMDS layer is very thin and colorless, like other organosilicon compounds, the observed contrast and color of the MoS₂ flake on the ultra-thin HMDS layer do not differ much from that on bare SiO₂. Fig. 1(b) shows the schematic of the device. Two probe con-

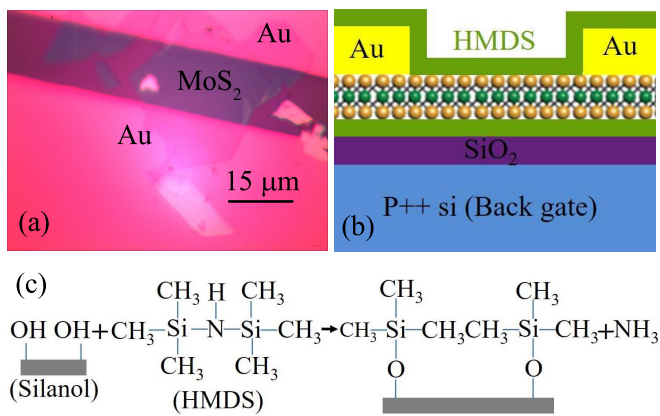


FIG. 1: (a) shows an optical image of MoS₂ FET with HMDS encapsulation on SiO₂/Si substrate with gold contacts and (b) shows a schematic cross-section view of this device. (c) shows a diagrammatic illustration of the reaction between surface silanol groups and HMDS.

ductance of both type, with and without HMDS encapsulation, devices were measured at room temperature in a homemade vacuum cryostat. A 10 kΩ series resistance was connected with the gate voltage V_g supply, which was controlled by a data acquisition card using a Lab-View program. The electrical measurements of without HMDS encapsulation device was done in vacuum in 10^{-4} mbar range, whereas the HMDS encapsulated device was measured in the ambient conditions by keeping the cryostat cover open. The two probe transport used a drain-source voltage bias V_{ds} controlled by a data acquisition card while the drain current I_d was measured through the voltage across a small bias-resistor, in series with the device, using a differential amplifier.

Thermally grown SiO₂ is an amorphous solid with dangling bonds and adsorbates acting as charge traps. When MoS₂ is placed on this surface, the interface trap states, which form within an accessible energy range of the channel's chemical potential, can change their occupancy and shield the gate electric field. Many different adsorbates can adhere to SiO₂. For instance, hydroxyl groups (-OH) pair with the surface-bound silicon's dangling bonds to form a layer of silanol (Si-OH) groups [26] that can act as electron traps. The silanol group can also do charge transfer with the MoS₂ via dipolar molecules such as water. Due to OH-termination, silanol is hydrophilic. Water molecules easily connect to the hydrogen of these silanol groups. Though some of the water molecules on the top surface of MoS₂ can be removed by vacuum annealing, a mono-layer or sub-mono-layer of hydrogen-bonded water cannot be extracted by pumping over long periods of time at room temperature [26, 27].

HMDS is a hydrophobic and air-stable organosilicon compound with the molecular formula $[(\text{CH}_3)_3\text{Si}]_2\text{NH}$, which is a derivative of ammonia with trimethylsilyl

groups in place of two hydrogen atoms [28, 29]. When HMDS is coated on the defective SiO₂ surface, the CH₃ in HMDS is covalently bonded with Si-OH [30] and forms organosilyl by replacing the hydrogen of the free Si-OH group with organosilyl groups. The covalent reaction between the HMDS and surface silanol groups is shown in Fig.1(c). Thus, the SiO₂ surface becomes hydrophobic due to the HMDS molecules, leaving no hydroxyl group available to form hydrogen bonds with water molecules.

Figure 2 compares the Raman spectra of single-layer MoS₂ on SiO₂/Si with and without HMDS encapsulation. The two characteristic Raman peaks, namely E_{2g}^1 and A_{1g} occur at 385.4 cm^{-1} and at 404 cm^{-1} , respectively, for both cases, leading to a peak frequency separation of 18.6 cm^{-1} . This corresponds to single-layer MoS₂ as reported in literature [31, 32]. The location of both

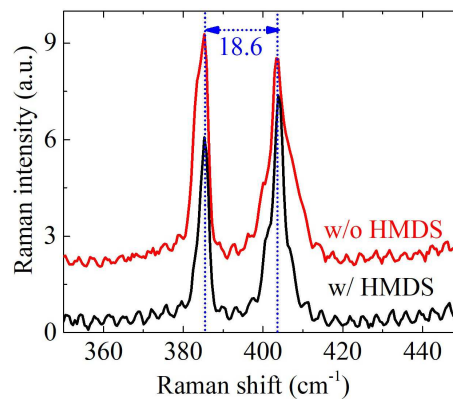


FIG. 2: Raman spectra of single-layer MoS₂ on SiO₂ with and without HMDS encapsulation showing sharpening of the Raman peaks resulting from the encapsulation.

the peaks in the HMDS-encapsulated MoS₂ layer remains same as that without HMDS within the experimental resolution. More significantly, in the HMDS-encapsulated MoS₂ layer, the full-width at half-maximum (FWHM) of the E_{2g}^1 and A_{1g} peaks dropped from 4.15 cm^{-1} to 2.08 cm^{-1} and from 4.15 cm^{-1} to 2.93 cm^{-1} , respectively. This suggests passivation of interface trap/defect states by HMDS as the interaction between the defect-bound excitons and phonons contributes to such line broadening.

Figure 3(a) shows the $I_d - V_g$ curves of the few-layer MoS₂ devices with, and without, HMDS passivation. The increase in I_d with increasing V_g indicates that both devices exhibit the n-type conduction above certain threshold gate-voltage V_{th} . The transfer characteristics without HMDS encapsulation, shown by the red curve in Fig. 3(a), exhibits a large hysteresis, even in vacuum, with V_{th} that differ by $\Delta V_{th} = 82 \text{ V}$ during forward and reverse sweeps of V_g . This large hysteresis is attributed to the charge-traps at the interface between MoS₂ and SiO₂ [33–36]. The areal density of the slow-traps responsible for this observed hysteresis is estimated using

$n_{\text{str}} = C_{\text{ox}}\Delta V_{\text{th}}/e$. Here, e is the magnitude of electronic charge and $C_{\text{ox}} = 12.1 \text{ nFcm}^{-2}$ is the per-unit-area capacitance of SiO_2 layer. This leads to $n_{\text{str}} = 6.2 \times 10^{12} \text{ cm}^{-2}$.

The sub-threshold swing, defined as $\text{SS} = 1/(d \log I_d/dV_g)$ just above V_{th} , is calculated to be 2.9 V/dec for the device without HMDS. This is from the inverse of the slope of the blue dashed line in Fig.3(a) for the backward gate sweep. This SS can be used to estimate the density of states (DOS) g_{ftr} of the fast-traps using $\text{SS} = k_b T \ln 10(1 + \gamma_{\text{ftr}})$. Here, $\gamma_{\text{ftr}} = e^2 g_{\text{ftr}}/C_{\text{ox}}$ is the ratio of the traps' quantum capacitance to the gate-oxide capacitance. This yields $g_{\text{ftr}} = 3.5 \times 10^{12} \text{ eV}^{-1}\text{cm}^{-2}$ for the device without HMDS.

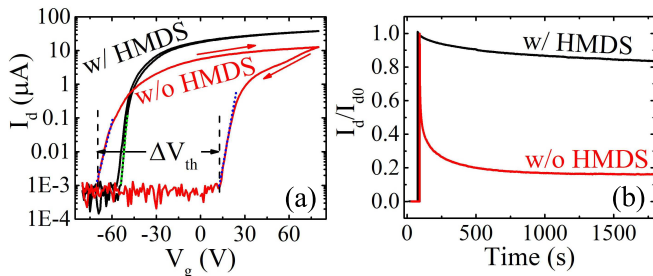


FIG. 3: (a) $I_d - V_g$ transfer characteristics of MoS_2 FET at $V_{\text{ds}} = 1 \text{ V}$ with and without HMDS passivation. (b) The time-dependent I_d of MoS_2 FET with and without HMDS passivation when V_g is quickly altered from -80 to $+80 \text{ V}$ at $t = 70 \text{ s}$ and 80 s , respectively. The y-axis is normalized to show both the curves on the same plot.

The solid black line in Fig.3(a) is the transfer characteristic of the HMDS encapsulated device measured in ambient conditions. It is noteworthy that even in ambient conditions and over the same V_g -sweep range and rate, the hysteresis is negligible. The ΔV_{th} is reduced from 82 V to a mere 3 V, corresponding to a reduction in slow traps' density to $2.2 \times 10^{11} \text{ cm}^{-2}$ i.e. more than 25 factor reduction as compared to the device without HMDS encapsulation. Further, the SS decreases from 2.9 V/dec to 0.9 V/dec, amounting to a fast trap DOS of $1.1 \times 10^{12} \text{ eV}^{-1}\text{cm}^{-2}$, i.e. more than three factor reduction. Thus, the HMDS encapsulation significantly helps in passivating the interface traps as well as gate bias stress due to ambient species. Although the extracted SS value is far from the temperature-limited lowest value, i.e. 60 mV/dec with no traps, it is one of the lowest values for the 300 nm SiO_2 gate. Note that for a fixed trap DOS, the SS value can also be reduced by increasing the gate capacitance.

Figure 3(b) shows I_d plots, scaled with their respective peak values, for the two devices as a function of time when V_g undergoes a step change from -80 to $+80 \text{ V}$. V_g was held at -80 V for 1 hour to achieve equilibrium between the chemical potential of the trap states and that of the channel. At this step rise in V_g from -80V to 80V ,

the I_d has step rise, in both the devices, due to a sudden rise of carrier density in the channel. This is followed by an abrupt decrease in I_d , especially in device without HMDS encapsulation, followed by a slow decrease in I_d due to the charging of the interface traps. The I_d of the unpassivated device decreases by almost 85% of its value immediately after the voltage step, whereas the passivated device only shows a 16% reduction, over 30 min time. This indicates a large areal density of traps, which capture the electrons from the channel, in the unpassivated device, leading to significant shielding of the back-gate electric field, as compared to the HMDS encapsulated device.

Figure 4 shows the field-effect mobility μ_{FE} of the MoS_2 FETs as a function of V_g with and without HMDS encapsulation with a marked difference between the two. The μ_{FE} is extracted from the transfer characteristics using the definition $\mu_{\text{FE}} = \left(\frac{L}{WC_{\text{ox}}V_d}\right) \left(\frac{dI_d}{dV_g}\right)$. Here, W and L are the channel width and length, respectively. Note that the maximum field-effect mobility of the HMDS encapsulated device is about 3.5 times of that of the unpassivated device. Note also the abrupt jumps in the μ_{FE} of the device without HMDS, presumably due to a large number of traps changing their charge state at certain V_g values, while μ_{FE} for device with HMDS is rather smooth.

The above μ_{FE} ignores the effect of the quantum capacitance of the channel C_{ch} and that of the interface traps C_{tr} . If one incorporates these, the change in channel carrier density, in response to ΔV_g change in the gate voltage, is given by $\Delta n = \left(\frac{C_{\text{ox}}\Delta V_g}{e}\right) \left(\frac{C_{\text{ch}}}{C_{\text{ch}}+C_{\text{ox}}+C_{\text{tr}}}\right)$. This will lead to a more appropriate mobility expression $\mu = e^{-1} \left(\frac{dG}{dn}\right)$ with G as the channel conductivity, which will differ from μ_{FE} by $\left(\frac{C_{\text{ch}}}{C_{\text{ch}}+C_{\text{ox}}+C_{\text{tr}}}\right)$ factor. Thus μ_{FE} will correspond to the actual mobility in the limit $C_{\text{ch}} \gg C_{\text{tr}}, C_{\text{ox}}$. This can be expected to be the case close to the degenerate limit. Thus μ_{FE} can be assumed to be close to the actual mobility for large $(V_g - V_{\text{th}})$ values.

The overall dependence of mobility on the carrier density also reflects the nature of the carrier scattering. The scattering can occur from the Coulomb potential of the interface traps, phonons and other excitations, as well as from the intrinsic defects. For a Coulomb scatterer one can write $G \propto n^\alpha$. Here, $1 \leq \alpha \leq 2$ is a parameter that depends on the screening of the Coulomb scatterer. For bare impurity Coulomb scattering, $\alpha = 2$ and for screened Coulomb impurity scattering $\alpha = 1$ [37, 38].

Close to the degenerate limit, n can be estimated as $n = C_{\text{ox}}(V_g - V_{\text{th}})/e$. With $G \propto I_d$, the slope of the $\ln(I_d) - V_s - \ln(V_g - V_{\text{th}})$ plot for large V_g can be used as an estimate of α . From Fig. 4, $\alpha \sim 1.9$, i.e. nearly 2, for the device without HMDS encapsulation, while for the HMDS encapsulated device, $\alpha \sim 1.1$, i.e. nearly 1. This

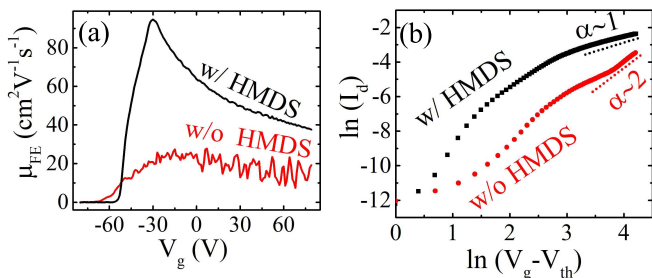


FIG. 4: (a) The field-effect mobility MoS₂ FET extracted from $I_d - V_g$ curves with and without HMDS passivation. (b) Variation of I_d with $V_g - V_{th}$ for MoS₂ FET with and without HMDS passivation.

analysis suggests that the HMDS encapsulation, or just the reduction in traps' density due to HMDS, reduces the bare Coulomb impurity scattering, presumably due to the reduction in interface traps, as compared to the screened impurity scattering.

A 2D semiconductor FET with its exposed channel to ambient air can accumulate more traps with time degrading device performance and causing threshold voltage instability. Besides these traps, there are also water and oxygen molecules in the environment that are absorbed depending on V_g value and cause the gate bias stress and lead to increased hysteresis. The latter is clearly insignificant in HMDS encapsulated device operated in air, as seen above, ruling out the gate bias stress. Further, the transfer characteristics of the HMDS encapsulated device, measured on the first day and after 25 days of keeping the device in air, are shown in Fig.5(a). There is negligible variation in the hysteresis window, a slight decrease in the current value, and a slight increase in the threshold voltage. The extracted μ_{FE} in Fig.5(b), indicates a mere 10% reduction after 25 days. This indicates that the top HMDS also protects MoS₂ channel quite well from the environmental oxygen and water molecules.

In conclusion, there is a substantial decrease in interface trap density and gate bias stress leading to an improved and lasting performance of MoS₂/SiO₂ FETs by HMDS encapsulation through interface passivation and top protection. A 25 factor reduction in slow traps' density, three times reduction in subthreshold swing and a significant improvement in the field-effect mobility is found in MoS₂ FET after HMDS encapsulation. The encapsulation method, based on spin coating of the chemically inert HMDS, is simple, scalable and can be extended to other 2D materials.

[1] Z. Zhou, and Y. K. Yap, "Two-dimensional electronics and optoelectronics: present and future Electronics", *Electronics* **6**, 53 (2017).

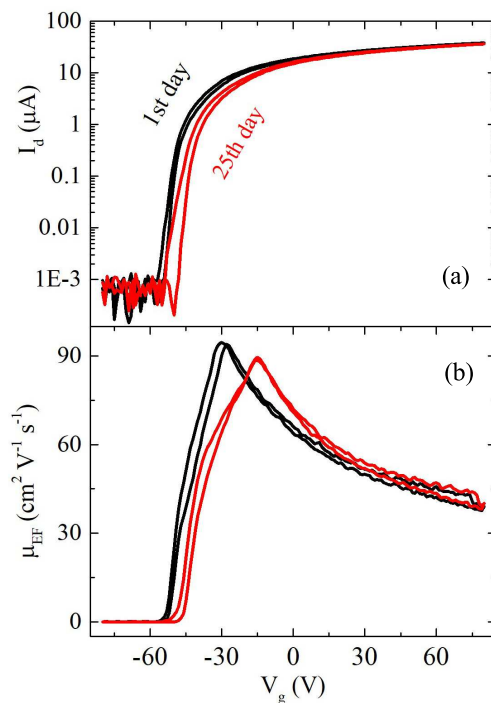


FIG. 5: (a) Transfer characteristics of HMDS-passivated MoS₂ FET measured on 1st and 25th day. (b) The field-effect mobility extracted from $I_d - V_g$ curves of (a).

- [2] K. F. Mak, C. Lee, J. Hone, J. Shan, and T. F. Heinz, "Atomically thin MoS₂: a new direct-gap semiconductor", *Phys. Rev. Lett.* **105**, 136805 (2010).
- [3] B. Radisavljevic, A. Radenovic, J. Brivio, V. Giacometti, and A. Kis, "Single-Layer MoS₂ Transistors", *Nat. Nanotechnol.* **6**, 147 (2011).
- [4] Y. Yoon, K. Ganapathi, and S. Salahuddin, "How Good Can Monolayer MoS₂ Transistors Be? ", *Nano Lett.* **11**, 3768 (2011).
- [5] L. M. Martinez, N. J. Pinto, C. H. Naylor, and A. T. Johnson, "MoS₂ based dual input logic AND gate", *AIP Adv.* **6**, 125041 (2016).
- [6] S. Wachter, D. K. Polyushkin, O. Bethge, and T. Mueller, "A microprocessor based on a two-dimensional semiconductor", *Nat. Commun.* **8**, 14948 (2017).
- [7] D. Krasnozhan, D. Lembke, C. Nyffeler, Y. Leblebici, and A. Kis, "MoS₂ Transistors Operating at Gigahertz Frequencies", *Nano Lett.* **14**(10), 5905 (2014).
- [8] B. Radisavljevic, M. B. Whitwick, and A. Kis, "Integrated Circuits and Logic Operations Based on Single-Layer MoS₂", *ACS Nano* **5**(12), 9934 (2011).
- [9] O. L. Sanchez, D. Lembke, M. Kayci, A. Radenovic, and A. Kis, "Ultrasensitive photodetectors based on monolayer MoS₂", *Nat. Nanotechnol.* **8**, 497 (2013).
- [10] K. F. Mak, K. He, J. Shan, and T. F. Heinz, "Control of valley polarization in monolayer MoS₂ by optical helicity", *Nat. Nanotechnol.* **7**, 494 (2012).
- [11] O. L. Sanchez, E. A. Llado, V. Koman, A. F. Morral, A. Radenovic, and A. Kis, "Light generation and harvesting in a van der Waals heterostructure", *ACS Nano* **8**, 3042 (2014).
- [12] M. L. Tsai, S. H. Su, J. K. Chang, D. S. Tsai, C. H. Chen,

- C. I. Wu, L. J. Li, L. J. Chen, and J. H. He, "Mono-layer MoS₂ heterojunction solar cells", *ACS Nano* **8**(8), 8317 (2014).
- [13] Z. Yu, Z. Y. Ong, S. Li, J. B. Xu, G. Zhang, Y. W. Zhang, Y. Shi, and X. Wang, "Analyzing the Carrier Mobility in Transition-Metal Dichalcogenide MoS₂ Field-Effect Transistors", *Adv. Funct. Mater.* **27**(19), 2017, 1604093.
- [14] L. Cheng, and Y. Liu, "What Limits the Intrinsic Mobility of Electrons and Holes in Two Dimensional Metal Dichalcogenides? ", *J. Am. Chem. Soc.* **140**(51), 17895-17900 (2018).
- [15] D. J. Late, B. Liu, H. S. S. R. Matte, V. P. Dravid, and C. N. R. Rao, "Hysteresis in Single-Layer MoS₂ Field Effect Transistors", *ACS Nano* **6**, 5635-5641 (2012).
- [16] T. Li, G. Du, B. Zhang, and Z. Zeng, "Scaling behavior of hysteresis in multilayer MoS₂ field effect transistors", *Appl. Phys. Lett.* **105**, 093107 (2014).
- [17] Y. Guo, X. Wei, J. Shu, B. Liu, J. Yin, C. Guan, Y. Han, S. Gao, and Q. Chen, "Charge trapping at the MoS₂-SiO₂ interface and its effects on the characteristics of MoS₂ metal-oxide-semiconductor field effect transistors", *Appl. Phys. Lett.* **106**, 103109 (2015).
- [18] K. Cho, W. Park, J. Park, H. Jeong, J. Jang, T. Y. Kim, W. K. Hong, S. Hong, and T. Lee, "Electric Stress-Induced Threshold Voltage Instability of Multilayer MoS₂ Field Effect Transistors", *ACS Nano* **7**, 7751-7758 (2013).
- [19] S. Y. Kim, S. Park, W. Choi, "Enhanced carrier mobility of multilayer MoS₂ thin-film transistors by Al₂O₃ encapsulation", *Appl. Phys. Lett.* **109**, 152101 (2016).
- [20] T. Li, B. Wan, G. Du, B. Zhang, Z. Zeng, "Electrical performance of multilayer MoS₂ transistors on high-k Al₂O₃ coated Si substrates", *AIP Adv.* **5**, 057102 (2015).
- [21] H. Liu, and D. Y. Peide, " MoS₂ dual-gate MOSFET with atomic-layer-deposited Al₂O₃ as top-gate dielectric", *IEEE Electron Device Lett.* **33**:546-8 (2012).
- [22] D. Kufer, G. Konstantatos, "Highly sensitive, encapsulated MoS₂ photodetector with gate controllable gain and speed", *Nano Lett.* **15**:7307-13 (2015).
- [23] G. H. Lee, X. Cui, Y. D. Kim, G. Arefe, X. Zhang, C. H. Lee, F. Ye, K. Watanabe, T. Taniguchi, P. Kim, and J. Hone, "Highly stable, dual-gated MoS₂ transistors encapsulated by hexagonal boron nitride with gate-controllable contact, resistance, and threshold voltage", *ACS Nano*, **9**:7019-26 (2015).
- [24] W. Bao, X. Cai, D. Kim, K. Sridhara, M. S. Fuhrer, "High mobility ambipolar MoS₂ field-effect transistors: Substrate and dielectric effects", *Appl. Phys. Lett.* **102**, 042104 (2013).
- [25] A. C. Gomez, M. Buscema, R. Molenaar, V. Singh, L. Janssen, H. S. Van Der Zant, and G. A. Steele, "Deterministic transfer of two-dimensional materials by all-dry viscoelastic stamping", *2D Mater.* **1**, 011002 (2014).
- [26] See page 62 of R. K. Iler, *The Chemistry of Silica* (Wiley-Interscience, New York, 1979).
- [27] K. Nagashio, T. Yamashita, T. Nishimura, K. Kita, and A. Toriumi, "Electrical transport properties of graphene on SiO₂ with specific surface structures", *J. Appl. Phys.* **110**, 024513 (2011).
- [28] R. C. Osthoff, S. W. Kantor, "Organosilazane Compounds", *Inorganic Syntheses* **5**, 55-64 (1957).
- [29] N. Tasaltin, D. Sanli, A. Jonáš, A. Kiraz, and C. Erkey, "Preparation and characterization of superhydrophobic surfaces based on hexamethyldisilazane-modified nanoporous alumina", *Nanoscale Research Letters* **6**, 1-8 (2011).
- [30] Y. Yuan, Y. Chen, W. L. Chen, R. J. Hong, "Preparation, durability and thermostability of hydrophobic antireflective coatings for solar glass covers", *Solar Energy* **118**, 222-231 (2015).
- [31] C. Lee, H. Yan, L. E. Brus, T. F. Heinz, J. Hone, and S. Ryu, "Anomalous Lattice Vibrations of Single and Few-Layer MoS₂", *ACS Nano* **4**(5), 2695 (2010).
- [32] A. C. Gomez, N. Agrait, and G. R. Bollinger, "Optical identification of atomically thin dichalcogenide crystals", *Appl. Phys. Lett.* **96**, 213116 (2010).
- [33] A. K. Singh, and A. K. Gupta, "Reversible control of doping in graphene-on-SiO₂ by cooling under gate-voltage", *J. Appl. Phys.* **122**, 195305 (2017).
- [34] D. J. Late, B. Liu, H. S. S. R. Matte, V. P. Dravid, and C. N. R. Rao, "Hysteresis in Single-Layer MoS₂ Field Effect Transistors", *ACS Nano* **6**(6), 5635 (2012).
- [35] Y. Guo, X. Wei, J. Shu, B. Liu, J. Yin, C. Guan, Y. Han, S. Gao, and Q. Chen, "Charge trapping at the MoS₂-SiO₂ interface and its effects on the characteristics of MoS₂ metal-oxide semiconductor field effect transistors", *Appl. Phys. Lett.* **106**, 103109 (2015).
- [36] S. P. Jana, S. Gupta, and A. K. Gupta, "Blocking transition of interface traps in MoS₂/SiO₂ field-effect transistors", *Phys. Rev. B* **108**, 195411 (2023).
- [37] S. Adam, and S. D. Sarma, "Boltzmann transport and residual conductivity in bilayer graphene", *Phys. Rev. B* **77**, 115436 (2008).
- [38] M. P. Lilly, J. L. Reno, J. A. Simmons, I. B. Spielman, J. P. Eisenstein, L. N. Pfeiffer, K. W. West, E. H. Hwang, and S. D. Sarma, "Resistivity of dilute 2D electrons in an undoped GaAs heterostructure", *Phys. Rev. Lett.* **90**, 056806 (2003).